Accepted Manuscript

Alkane-grown *Beauveria bassiana* produce mycelial pellets displaying peroxisome proliferation, oxidative stress, and cell surface alterations

Carla Huarte-Bonnet, Flávia R.S. Paixão, Juan C. Ponce, Marianela Santana, Eduardo D. Prieto, Nicolás Pedrini

PII: S1878-6146(17)30126-5

DOI: 10.1016/j.funbio.2017.09.003

Reference: FUNBIO 849

To appear in: *Fungal Biology*

Received Date: 20 July 2017

Revised Date: 8 September 2017

Accepted Date: 21 September 2017

Please cite this article as: Huarte-Bonnet, C., Paixão, F.R.S., Ponce, J.C., Santana, M., Prieto, E.D., Pedrini, N., Alkane-grown *Beauveria bassiana* produce mycelial pellets displaying peroxisome proliferation, oxidative stress, and cell surface alterations, *Fungal Biology* (2017), doi: 10.1016/j.funbio.2017.09.003.

Fungal Biology, special issue 'Biology of Fungal Systems under Stress'

Alkane-grown *Beauveria bassiana* produce mycelial pellets displaying peroxisome proliferation, oxidative stress, and cell surface alterations

Carla Huarte-Bonnet[1], Flávia R.S. Paixão[1], Juan C. Ponce[1], Marianela Santana[1], Eduardo D. Prieto[2], Nicolás Pedrini[1*]

[1]Instituto de Investigaciones Bioquímicas de La Plata (INIBIOLP), CCT La Plata Consejo Nacional de Investigaciones Científicas y Técnicas (CONICET) - Universidad Nacional de La Plata (UNLP), calles 60 y 120, 1900 La Plata, Argentina.

[2]Instituto de Investigaciones Fisicoquímicas Teóricas y Aplicadas (INIFTA), CCT La Plata Consejo Nacional de Investigaciones Científicas y Técnicas (CONICET) - Universidad Nacional de La Plata (UNLP) – Sucursal 4 Casilla de Correo 16, 1900 La Plata, Argentina.

* Address for correspondence: npedrini@med.unlp.edu.ar ; Tel. +542214241596 ext 383; Fax +542214258988

Abstract

The entomopathogenic fungus *Beauveria bassiana* is able to grow on insect cuticle hydrocarbons as the sole carbon source, inducing several enzymes involved in alkane assimilation and concomitantly increasing virulence against insect hosts. In this study, we describe some physiological and molecular processes implicated in growth, nutritional stress response, and cellular alterations found in alkane-grown fungi. The fungal cytology was investigated using light and transmission electron microscopy (TEM) while the surface topography was examined using atomic force microscopy (AFM). Fungal hydrophobicity was also measured on the cell surface. Additionally, the expression pattern of several genes associated with oxidative stress, peroxisome biogenesis, and hydrophobicity were analysed by qPCR. We found a novel type of growth in alkane-cultured *B. bassiana* similar to mycelial pellets described in other alkane-free fungi, which were able to germinate and produce viable conidia in media without a carbon source and to be pathogenic against larvae of the beetles *Tenebrio molitor* and *Tribolium castaneum*. Optical microscopy and TEM showed that pellets were formed by hyphae cumulates with high peroxidase activity, exhibiting peroxisome proliferation and an apparent surface thickening. Alkane-grown conidia appeared to be more hydrophobic and cell surfaces displayed different topography than glucose-grown cells, as it was observed by AFM. We also found a significant induction in several genes encoding for peroxins, catalases, superoxide dismutases, and hydrophobins. These results show that both morphological and metabolic changes are triggered in mycelial pellets derived from alkane-grown *B. bassiana*.

Keywords: entomopathogenic fungi, hydrocarbon degradation, hydrophobicity, peroxins.

Introduction

Entomopathogenic fungi do not require any specialized mode of entry to invade their insect hosts; they usually start the infection cycle by penetrating through the insect epicuticle. This outermost cuticle layer is composed by lipids, mostly aliphatic hydrocarbons or alkanes with both straight-chain and methyl-branched, usually between 20 to more than 40 carbons (Pedrini et al., 2007). The ability of entomopathogenic fungi to degrade insect hydrocarbons and utilize them for energy production and for the biosynthesis of cellular components was first shown in *Beauveria bassiana* and *Metarhizium anisopliae* (Napolitano and Juárez, 1997). In addition, alkane-grown *B. bassiana* was more virulent than glucose-grown fungi by producing either higher insect mortality or lesser mean lethal time against different hosts (Crespo et al. 2002; Pedrini et al. 2009). Thus, alkane degradation by *B. bassiana* represents a key metabolic pathway related to the insect pathogenic nature of the fungus. However, growth on alkanes causes major changes in fungal metabolism (Crespo et al., 2000) and a scenario of oxidative stress is caused by the accumulation of reactive oxygen species, which is successfully overcome by the induction of antioxidant genes and enzymes (Huarte-Bonnet et al., 2015). Moreover, the spore yields in alkane-grown fungi are usually lower than those obtained in fungi grown in rich media (Napolitano and Juárez, 1997), impairing the achievement for acceptable mass production in industrial resources.

Filamentous fungi often grow in liquid cultures exhibiting a plethora of morphological structures, e.g. three-dimensional aggregates ranging from loose clumps of mycelia to dense pellets. Pellet growth seems favorable for the production of several biotechnological products, and the optimizations of pellets formation are constantly revised

(Wucherpfenning et al., 2010). In this regard, cell aggregation is dependent on several cultivation conditions like the initial particle concentration, the hydrodynamic conditions, and the pH value, among other factors (Grimm et al., 2005a). As far as we know, there are no reports about pellet formation in alkane-grown fungi. The aim of the current study was to characterise a novel type of cellular growth produced in alkane-cultured *B. bassiana*, similar to mycelial pellets described in other filamentous fungi. We described an oxidative stress scenario associated with peroxidase activity and peroxisome proliferation, the same as cell surface alterations in alkane-grown *B. bassiana*.

Materials and methods

~~***Cultivation of fungi***~~

Fungal cultivation and inoculants preparation

Beauveria bassiana strain GHA was routinely cultured and maintained on potato dextrose agar (PDA) (BD Difco, Sparks, USA). Conidia harvested from this medium were suspended in 0.01% Tween 80 in sterile distilled water, vortexed for approximately 3 min, and filtered through a 75 µm sieve to remove debris. These conidial suspensions were adjusted in a Neubauer chamber to 1×10^7 conidia ml^{-1}, and were used to inoculate complete liquid medium (CM) flasks and incubated at 26ºC for 2 days with aeration (180 rpm). CM is composed by 0.4 g KH_2PO_4, 1.4 g Na_2HPO_4, 0.6 g $MgSO_4.7H_2O$, 1.0 g KCl, 0.7 g $NH_4NO_3.7H_2O$, 10 g glucose, and 5 g yeast extract in 1,000 ml of distilled water. Fungi were harvested by centrifugation for 20 min at 7200×g, washed with sterile water, weighted and used as initial inoculums to grow under the same conditions for additional 3,

5 and 7 days in both CM and minimal liquid medium (MM) supplemented with *n*-hexadecane (MM-C16). MM is composed of CM without the glucose and yeast extract, and MM-C16 is MM supplemented with *n*-hexadecane (Sigma-Aldrich, USA) (C16, 1% final concentration) as previously described (Pedrini et al., 2010).

~~Conidia suspensions were inoculated in CM flasks and incubated at 26ºC for 2 days with aeration (180 rpm). Fungi were harvested and grown under the same conditions for additional 3 and 7 days in CM and MM-C16~~. Mycelia and conidia (referred from now on as biomass) were obtained by pellet centrifugation for 20 min at 7200×g. The remaining fungal cells that were found in close contact with the alkane interface in the supernatant were isolated from the media culture by filtration and are referred from now on as mycelial pellets. All cell samples were washed with sterile water. At each time period, pH was measured on the remaining media, and humid biomass was weighted. Humid biomass ratio was calculated as humid final biomass/initial inoculum mass.

Microbial adhesion to hydrocarbons (MATH) assay

Cell surface hydrophobicity was determined as Holder et al. (2007). Briefly, conidia obtained in CM and MM-C16 after 3, 5, and 7 days were washed in PUM buffer (per litre: 22.2 g K_2HPO_4, 7.26 g KH_2PO_4, 1.8 g urea, 0.2 g $MgSO_4$. $7H_2O$, final pH 7.1). Fungal cell suspensions were adjusted to OD_{470} 0.4 and dispensed into acid-washed glass tubes. Hexadecane was then added to each tube and samples were vortexed three times for 30 s each. The tubes were then incubated at 4ºC for 10 min and after removal of the *n*-hexadecane solid phase the density of the resultant cell suspension determined in a spectrophotometer at 470nm. The hydrophobic index was calculated using the following

105 equation: ($A_{470,\ control}$-$A_{470,\ hexadecane\ treated}$)/($A_{470,\ control}$). Four biological replicates with five
106 repetitions each were measured.

107 ***Microscopy images***

108 For optical and transmission electron microscopy (TEM) images, seven day cultures
109 from CM, MM-C16, and mycelial pellets were used. Fresh samples were observed with a
110 Nikon eclipse e200 optical microscope (Nikon Corp., Japan). For TEM, samples were
111 washed and fixed in glutaraldehyde 2% for 2 h with soft vacuum, then washed three times
112 with phosphate buffer (pH 7.2-7.4). Postfixation was performed with 1% osmium tetroxide
113 at 4ºC for 1 h, followed by dehydration with a series of alcohols in a vacuum chamber.
114 Samples were finally infiltrated with epoxy resin and thin sections of approximately 70 nm
115 were cut. TEM observation was made in a JEM 1200 EX II (JEOL Ltd., Japan). For 3,3-
116 diaminobenzidine (DAB) (Sigma-Aldrich, USA) staining, an additional staining overnight
117 with DAB was included in both fresh and fixated samples with glutaraldehyde 2%. In order
118 to characterise the cell topography of fungi grown on CM and MM-C16, atomic force
119 microscopy (AFM) images from 5 d conidia were obtained in air, using a MultiMode
120 Scanning Probe Microscope (Veeco, USA) equipped with a Nanoscope V controller
121 (Veeco). All measurements were obtained with Tapping® mode, using probes doped with
122 silicon nitride (RTESP, Veeco with tip nominal radius of 8-12 nm, 271-311 kHz, force
123 constant 20-80 N/m). Typical rate scanners were 1Hz. Fungal cells were placed on 0.22 μm
124 pore-size Millipore filters and air-dried before examination.

125 ***Mycelial pellets viability and pathogenicity***

126 Sporulation and viability of 7 d mycelial pellets were assessed as follows: fungal
127 propagules were placed in Petri plates and held for 5 d at 4ºC in a desiccator with activated
128 silica gel until moisture content was reduced to ≤ 5% (w/w). Then, 30 mg of dried pellets
129 were cultured in agar-agar media with ampicillin for 14 d at 26ºC, growth was monitored
130 daily and conidia produced were harvested with sterile water. Conidial production from the
131 suspension was determined with a Neubauer chamber, calculated as total conidia/ initial
132 dried pellet mass. To establish conidial viability, the suspension was also used to inoculate
133 CM-agar plates and germination was monitored and calculated after 24 h at 26ºC. For each
134 replicate, 300 conidia were studied, and germination was calculated as 100 × germinated
135 conidia/total conidia. For these tests, five replicates were done.

136 For pathogenicity assays, three groups of 10 larvae of each *T. castaneum* and *T.*
137 *molitor* were placed in sterile plates containing a mixture of fresh 7 d mycelial pellets and
138 humid vermiculite, prepared as follows: 0.325 g of mycelial pellets were placed in a sterile
139 plate with 1.5 ml of sterile water, then 1.75 g of sterile vermiculite was added and mixed
140 gently with a sterile spatula. Control plates were similarly prepared without the mycelial
141 pellets. Beetles were maintained at 26ºC and 70% RH. Mortality was checked every three
142 days and all dead larvae were removed after each count. Afterward, dead beetles were
143 washed in 70% ethanol for 30 s, rinsed in sterile distilled water for 2 min, allowed to dry,
144 and then placed in individual humid chambers at 25ºC to confirm fungal infection. The
145 experiment was repeated two more times. Mortality data were corrected for control
146 mortality using the Abbott's equation (Abbott, 1925).

147 ***Gene expression analysis***

Total RNA was extracted employing the RNAeasy Plant Mini kit (Qiagen, Germany), including an on-column DNA digestion step (Qiagen). RNA samples were quantified with a Nanodrop spectrophotometer (Thermo, USA), and the integrity was assessed on a 1% (w/v) agarose gel. Two-step real-time polymerase chain reaction (RT-PCR) was carried out with iScript cDNA Synthesis Kit and iQ SYBR Green Supermix (Bio-Rad, USA). Amplification was performed in an StepOne Plus equipment (Applied Biosystems, USA) employing 20 ng reverse transcribed total RNA for each sample. Primers corresponding to oxidative stress markers *Bbsod1*, *Bbsod2, Bbsod3, BbcatA, BbcatB, BbcatC, BbcatD, BbcatP, Bbgpx* and *Bbgst,* peroxisome biogenesis genes *Bbpex5, Bbpex7, Bbpex14/17 and Bbpex19,* and hydrophobicity related genes *Bbhyd1* and *Bbhyd2* were designed using Gene Runner program. In order to confirm that only single products were amplified, a temperature-melting step was then performed. The calibration curve method was used for the analysis of data obtained from the RT-PCR system, with gamma actin (*Bbact*) as the housekeeping gene. This gene was selected after a validation test with geNorm algorithm for several commonly used housekeeping genes; i.e., *Bb28, BbcypA, Bbtub, BbCrza, Bbact* and *Bbgpd* using Qbaseplus software (https://www.qbaseplus.com). Four independent biological replicates were tested, with technical duplicates for each sample. The relative expression ratio of each target gene was calculated with ΔΔCt approach in MM-C16 cells and mycelial pellets, using CM cells as control. Primers used, PCR efficiencies, and putative functions of the proteins encoded are listed in Table 1.

Statistical analysis

169 Differences among means were determined by two-way analysis of variance
170 (ANOVA) followed by the Tukey posttest, using GraphPad Prism (GraphPad Software
171 Inc., San Diego, CA).

172

173 **Results**

174 ***Fungal growth on hydrocarbons***

175 After three days of culture with vigorous agitation, several macroscopic, spherical,
176 non-uniform size aggregates appeared in C16-added MM (Fig. 1A). These aggregates were
177 found in close contact with the hydrocarbon phase (they could not be isolated from the
178 aqueous phase by centrifugation) but were not found in CM in the same growing
179 conditions. Humid biomass (fungal cells excluding the mycelial pellets) and pH of the
180 media were monitored and results are shown in Table 2. In all cases, biomass ratio
181 ~~(calculated as humid final mass/initial inoculum mass)~~ was significantly lower ($p < 0.05$) in
182 MM-C16 than in CM. pH behavior appeared to be inverted for minimal and complete
183 cultures; cell-free MM-C16 had a decreased but not significant tendency in pH over days,
184 whereas cell-free CM increased pH significantly ($p < 0.01$).

185 ***Microbial adhesion to hydrocarbons (MATH) assay***

186 Conidia from CM and MM-C16 cultures were isolated after 3, 5, and 7 days. The
187 hydrophobic index (HI) for all samples is shown in Fig. 2. The HI from CM conidia
188 decreased from 0.62 (day 3) to 0.25 (day 7) ($p < 0.001$). On day 3, the HI was significantly

189 higher ($p < 0.05$) in CM conidia than in MM-C16 conidia. On the contrary, on day 5 the HI
190 was significantly higher ($p < 0.01$) in MM-C16 conidia than in CM conidia.

191 ***Microscopy images***

192 ~~After observation by optical microscopy, the spherical aggregates showed to be~~
193 ~~formed by hyphae cumulate.~~ Optical microscopy showed that the spherical aggregates are
194 formed by hyphal cumulates (Fig. 1B). Visible *n*-hexadecane droplets were found
195 surrounding the pellet surface (Fig. 1C). Alkane-grown mycelial pellets were also stained
196 with DAB, a chemical used for determining peroxidase activity, which is usually employed
197 as peroxisome marker (Fahimi, 2017). The hyphal cumulates appeared strongly stained,
198 different from hyphae close to the aggregate borders, which showed lower staining
199 reaction. (Figs. 1D, E).

200 Alkane-grown mycelial pellets were also processed and observed by TEM, the same
201 as fungal conidia and mycelia. The preparative section cuts from mycelial pellets were
202 previously analysed by optical microscopy (Fig. 3A), where spheres looked like low dense
203 clusters of fungal cells that might contain other compounds, like hydrocarbons, immersed
204 in their structure. In the fungal cells forming the hyphal aggregates, TEM images showed
205 surfaces with an irregular comb-like form facing the cytoplasm and small vesicles (Fig.
206 3B), the same as an apparent surface thickening (~ 0.36 µm) compared to MM-C16 (~ 0.15
207 µm) (Fig. 3C) and CM cells (~ 0.11 µm) (Fig. 3D). Images from DAB stained mycelial
208 pellets revealed higher peroxidase activity, visualized as small black dots due to DAB
209 reaction with H_2O_2, inside the cells and also in cellular interconnections; several
210 peroxisomes and clear hairpin-like structures in the cell surface were also observed (Figs.

211 3E, F). On the contrary, DAB staining CM cells revealed lower peroxidase activity, mainly
212 found in vacuoles, fewer or not clear mature peroxisomes and smooth cell surfaces (Figs.
213 3G, H).

214 AFM images were obtained for CM and MM-C16 conidia from 5-day cultures,
215 showing distinctive differences on cell surfaces. CM conidia displayed irregular forms and
216 different and variable diameters (between 1.5 and 5.4 μm) (Figs. 4A, C). On the contrary,
217 MM-C16 conidia looked like a spherical form, smaller, and homogeneous (between 0.9 and
218 2.5 μm) (Figs. 4B, D). Also, CM conidia showed distinctive topographical characteristics
219 with deep and rough edges, whereas MM conidia showed a more uniform structure (Figs.
220 4E, F).

221 ***Mycelial pellets viability and pathogenicity***

222 Dried mycelial pellets were cultured in agar-agar plates. Hyphal growth was visible
223 after two days and sporulation started on day 6. At day 14, conidia were harvested and
224 counted. Conidial production varied from 1×10^9 to 5×10^9 conidia per gram of dried pellet
225 and germination in CM plates was 99.7%. Pathogenicity bioassays were done with fresh 7
226 d mycelial pellets and results are shown in Table 3. At day 8, *T. castaneum* mortality was
227 67.3 ± 13.1 % ~~mortality~~ ~~in all replicates~~, whereas *T. molitor* reached 96.7 ± 1.9 % ~~at day 8~~.
228 These results showed that mycelial pellets are formed by active fungal cells, pathogenic
229 against beetle larvae, which can grow without an external carbon source producing viable
230 conidia.

231 ***Gene expression analysis***

Antioxidant stress-marker genes displayed different expression patterns in alkane-grown mycelial pellets (Fig. 5A). For the superoxide dismutase family, *Bbsod1* was induced on day 3 (6.1-fold induction), but not as significantly as on day 7. In contrast, *Bbsod3* was induced on day 3 and day 7 (1.7- and 4.9-fold induction, respectively). However, *Bbsod2* was not induced in the conditions tested. For the glutathione system, *Bbgst* showed little induction (3.4- and 1.8-fold on day 3 and day 7, respectively), and *Bbgpx* expression was reduced on day 3 (0.7-fold) and induced at day 7 (2.5-fold). For the catalase family, *Bbcatb* (4.9-fold expression at day 3), *Bbcatc* (4.2- and 4.7-fold on day 3 and day 7, respectively) and *Bbcatp* (14.8-fold and 4.3-fold on day 3 and day 7, respectively) were induced in alkane cultures. Moreover, the peroxisomal-protein encoding gene *Bbcatp* was significantly induced ($p < 0.01$) on day 3 compared with day 7.

In order to study the expression pattern of genes involved in the peroxisomes biosynthesis pathway, several genes encoding for PEX proteins were also measured by qPCR (Fig. 5B). Some *pex* genes were induced in mycelial pellets, as follows: *Bbpex7* (2.5-fold expression on day 3), *Bbpex14/17* (1.9-fold and 4.5-fold on day 3 and 7, respectively) and *Bbpex19* (2.8-fold and 3.9-fold on day 3 and 7, respectively). In contrast, *Bbpex7* and *Bbpex5* were not induced on day 7, and at both time periods, respectively.

To study candidate genes involved in cell surface hydrophobicity, hydrophobin genes were measured in mycelial pellets and MM-C16 biomass, using CM biomass as control (Fig. 5C). Although *Bbhyd1* and *Bbhyd2* genes were not induced in mycelial pellets, both genes were strongly induced on day 3 and day 7 in MM-C16 biomass. The transcripts levels of *Bbhyd1* were 22.8-fold induction and 5.8-fold induction on day 3 and day 7, respectively. For *Bbhyd2*, the expression level was 74.1-fold induction on day 3, and 13.9-

255 fold induction on day 7. Thus, gene expression for *Bbhyd2* at day 3 was significantly higher
256 ($p<0.001$) than on day 7.

257

258 **Discussion**

259 A novel type of growth was described in *B. bassiana* cultured in hexadecane-
260 supplemented liquid minimal media, consisting in hyphal aggregates similar to mycelial
261 pellets found in other filamentous fungi (Grimm et al., 2005a; Metz and Kossen, 1977).
262 However, *B. bassiana* pellets were found only in alkane-grown fungi but not in glucose-
263 grown cells. These complex structures resulted to be stable, spherical aggregates, formed
264 by branched and partially intertwined hyphae networks that were able to germinate and
265 produce viable conidia without an external carbon source. Preliminary pathogenity assays
266 showed that after one week, these propagules caused the death of mealworms and red flour
267 beetle larvae. Apart from the mycelial pellets development, no significant increment was
268 recorded in MM-C16 biomass during the entire incubation period; in contrast to CM
269 cultures, where biomass was more than 4 times higher than the initial inoculums. It has
270 been already reported that *B. bassiana* is capable of growing on media supplemented with
271 hydrocarbons; moreover, it was established that *n*-hexadecane was the preferred substrate
272 among several hydrocarbons tested (Huarte-Bonnet et al., 2017; Pedrini et al., 2010). Thus,
273 these results indicate that alkane-grown *B. bassiana* is actually under active division and
274 growth, but these new cells are forming mycelial pellets in the alkane interface and are not
275 part of the initial biomass.

Differences in ~~both~~ hydrophobic cell surface indexes ~~and pH pattern~~ were found in conidial cells isolated from CM and MM-C16 biomass. AFM images also showed topographical differences between CM and MM-C16 conidia. It is clear that the presence of *n*-hexadecane is triggering different cell responses in order to uptake this hydrophobic substrate. Although it is well established how *B. bassiana* degrade cuticular hydrocarbons (Pedrini et al., 2007; 2010; 2013), little is known about the mechanisms involved in the uptake of alkanes by entomopathogenic fungi. It is believed that different compounds are secreted or anchored to the fungal cell surface to internalize those carbon sources, as shown by TEM images in both conidia (Pedrini et al., 2007) and mycelial pellets (this study).

The present study also showed different pH patterns between CM and MM-C16 remaining liquid media. In this regard, secretion of acid compounds could be responsible for the acidification of the media observed in MM-C16 cultures. Oxalic acid was reported to be secreted by *B. bassiana* as a virulence factor against ticks, and its secretion was dependent on the media used (Kirkland et al., 2005). Also, alkane-assimilating microorganisms are known to secrete acid biosurfactants to facilitate hydrocarbon uptake; e.g., acidic sophorolipids, free fatty acids, among others (Kitamoto et al., 2002). Thus, it could be expected that similar compounds might be found in the remaining media of alkane-grown *B. bassiana*. ~~Differential pH in the remaining media and cell surface hydrophobicity might indirectly shed light to possible mechanisms of secretion and cell surface adaptation to hydrocarbon growth that is still to be discovered.~~ It was also previously shown that *B. bassiana*, neither *M. anisopliae* nor *Aspergillus niger*, strongly acidified the liquid minimal media supplemented with alkanes (Huarte-Bonnet et al., 2017). As pellet formation is highly regulated by pH in other filamentous fungi (Dynesen and

299 Nielsen, 2003; Glazebrook et al., 1992; Grimm et al., 2005b; Ryoo and Choi, 1999), pH
300 values might be either the cause or the consequence to pellet formation in alkane-grown *B.*
301 *bassiana.* Also, hydrophobins might play a role in hydrocarbons uptake. In this regard, we
302 found that though no induction was observed for *hyd* genes in mycelial pellets, MM-C16
303 biomass showed high expression of both *Bbhyd1* and *Bbhyd2*. However, hydrophobins play
304 a key role in pellet formation in *A. niger*, and hydrophobic interactions in the cell surface
305 were reported to favor the formation and stability of these aggregates (Dynesen and
306 Nielsen, 2003). These results suggest that although *hyd* genes are highly induced in *B.*
307 *bassiana* biomass immediately after contact with hydrocarbons, the mycelial pellets derived
308 from those cells did not express these genes since they might already have these proteins in
309 their surfaces. However, further assays to specifically detect hydrophobins in both fungal
310 cells are required to confirm this hypothesis.

311 An antistress response was triggered in mycelial pellets during growth on alkanes,
312 in coincidence with previous results obtained for MM-C16 biomass grown in similar
313 culture conditions (Huarte-Bonnet et al., 2015). In mycelial pellets, at least one gene of
314 each antistress response family was up-regulated at each time incubation period. Thus,
315 catalase and superoxide dismutase gene induction could also be used as clues for reactive
316 oxygen species localization, i.e., *Bbsod1* encodes for a Cu/Zn-dependent superoxide
317 dismutase localized in the cytoplasm (Xie et al., 2010) and *Bbsod3* encodes for a
318 mitochondrial Mn-isoform (Xie et al., 2012), whereas *Bbcatb, Bbcatc,* and *Bbcatp* encode
319 for cytoplasmic, secreted, and peroxisomal catalases, respectively (Wang et al., 2013). In
320 fact, the peroxisomal isoform was the most induced gene from the antistress response
321 system in mycelial pellets. However, gene expression data is not sufficient to fully

322 comprehend if the observed upregulation is useful to protect cells against potential
323 antagonists (both biotic and abiotic) or if it is a result to cells differentiation into mycelial
324 pellets, or both. Targeted single-gene knockout strategies and/or enzymatic studies in
325 subcellular fractions will be needed to confirm this point.

326 Peroxisomes are known to be the organelles where the last hydrocarbon degradation
327 reactions take place in *B. bassiana* (Pedrini et al., 2007). The biogenesis of peroxisomes
328 involves the action of several proteins, named peroxins, which are encoded by *pex* genes
329 (Li et al., 2016; Smith and Aitchison, 2013). In this study, *Bbpex7*, *Bbpex14/17,* and
330 *Bbpex19* were induced after 3 and/or 7 days of culture. In addition to gene expression
331 patterns, mycelial pellets staining reaction with DAB gave strongly brown stained cells
332 inside the pellet structure, but also inside the individual cells, indicating high
333 catalase/peroxidase activity and peroxisomal proliferation. Moreover, the high number of
334 small black dots found inside alkane-grown cells and the induction of *pex* genes are
335 suggesting that the peroxisome biogenesis pathway is being activated under this growth
336 condition, as it was reported for alkane-grown yeast (Fukui and Tanaka, 1979; Monosov et
337 al., 1996; Smith and Aitchison, 2013; Tanaka and Ueda, 1993).

338 We conclude that two cellular populations are present in fungi grown in liquid
339 minimal media supplemented with *n*-hexadecane. Both fungal propagules have different
340 molecular and physiological characteristics between them and also compared to cells grown
341 in rich media. In this sense, several unknown direct or indirect responses to hydrocarbon
342 supplementation might be acting as triggers to initiate pellet formation since they are not
343 present in rich media in the same incubation conditions. For other filamentous fungi, pellets
344 formation in liquid cultures are preferred for the non-vicuos rheology of the broth, better

mass transfer and easier pellet separation than with mycelial cultures (Wucherpfenning et al., 2010). In alkane-grown fungi, hydrocarbon droplets in liquid media might be acting as initial nucleation for pellets formation since these structures might assure fungal cells of an easy access to the hydrophobic carbon source in the interface. However, additional studies are needed to better understand the relationship between fungal metabolic adaptations in hydrocarbon-supplemented cultures and pellet formation.

Acknowledgments

We are grateful to Gabriel M. Mascarin for initial and helpful discussion about fungal pellets formation. We also thank Elsevier BV for sponsoring the International Symposium on Fungal Stress (ISFUS)-2017 Silver Award to CHB. This research was partially supported by grants from the Agencia Nacional de Promoción Científica y Tecnológica (PICT-2012-1964 and PICT-2015-2763), Argentina. The work was also facilitated by grants in support of the ISFUS-2017 meeting from the Coordenação de Aperfeiçoamento de Pessoal de Nível Superior (CAPES) of Brazil - PAEP 88881.123209/2016-01, by a grant from the Fundação de Amparo à Pesquisa do Estado de Goiás of Brazil – 201710267000110, and by a International Collaborative Research Grant between the Consejo Nacional de Investigaciones Científicas y Técnicas (CONICET) and the São Paulo Research Foundation (FAPESP) #2013/50518-6. NP is member of the CONICET Researcher's Career, Argentina.

References

Abbott WS, 1925. A method of computing the effectiveness of an insecticide. *Journal of Economical Entomology* **18**: 265-267.

Crespo R, Juárez MP, Cafferata LFR, 2000. Biochemical interaction between entomopathogenous fungi and their host-like hydrocarbons. *Mycologia* **92:** 528–536

Crespo R, Júrez MP, Dal Bello GM, Padín S, Fernández GC, Pedrini N, 2002. Increased mortality of *Acanthoscelides obtectus* by alkane-grown *Beauveria bassiana*. *BioControl* **47**: 685–696.

Dynesen J, Nielsen J, 2003. Surface hydrophobicity of *Aspergillus nidulans* conidiospores and its role in pellet formation. *Biotechnology Progress* **19**: 1049–1052.

Fahimi HD, 2017. Cytochemical detection of peroxisomes in light and electron microscopy with 3,3'-diaminobenzidine. *Methods in Molecular Biology* **1595**: 93-100.

Forlani L, Juárez MP, Lavarías S, Pedrini N, 2014. Toxicological and biochemical response of the entomopathogenic fungus *Beauveria bassiana* after exposure to deltamethrin. *Pest Management Science* **70**: 751-756.

Fukui S, Tanaka A, 1979. Peroxisomes of alkane- and methanol-grown yeast. Metabolic functions and practical applications. *Journal of Applied Biochemistry* **1**: 171-201.

Glazebrook MA, Vining LC, White RL, 1992. Growth morphology of *Streptomyces akiyoshiensis* in submerged culture: influence of pH, inoculum, and nutrients. *Canadian Journal of Microbiology* **38**: 98–103.

Grimm LH, Kelly S, Krull R, Hempel DC, 2005a. Morphology and productivity of filamentous fungi. *Applied Microbiology and Biotechnology* **69**: 375–384.

388 Grimm LH, Kelly S, Völkerding II, Krull R, Hempel DC, 2005b. Influence of mechanical
389 stress and surface interaction on the aggregation of *Aspergillus niger* conidia.
390 *Biotechnology and Bioengineering* **92**: 879–888.

391 Holder DJ, Kirkland BH, Lewis MW, Keyhani NO, 2007. Surface characteristics of the
392 entomopathogenic fungus *Beauveria (Cordyceps) bassiana*. *Microbiology* **153**: 3448–3457.

393 Huarte-Bonnet C, Juárez MP, Pedrini N, 2015. Oxidative stress in entomopathogenic fungi
394 grown on insect-like hydrocarbons. *Current Genetics* **61**: 289–297.

395 Huarte-Bonnet C, Kumar S, Saparrat M, Girotti JG, Santana M, Hallsworth JE, Pedrini N,
396 2017. Insights into hydrocarbon assimilation in eurotialean and hypocrealean fungi: roles
397 for CYP52 and CYP53 clans of cytochrome P450 genes. (sent for reviewing to *Applied*
398 *Biochemistry and Biotechnology*).

399 Kirkland BH, Eisa A, Keyhani NO, 2005. Oxalic acid as a fungal acaracidal virulence
400 factor. *Journal of Medical Entomology* **42**: 346-351.

401 Kitamoto D, Isoda H, Nakahara T, 2002. Functions and potential applications of glycolipid
402 biosurfactants–from energy-saving materials to gene delivery carriers–. *Journal of*
403 *Bioscience and Bioengineering* **94**: 187-201.

404 Li L, Wang J, Chen H, Gu Z, Wang Y, Sun G, 2016. Pex14/17, a filamentous fungi specific
405 peroxin, is required for import of peroxisomal matrix proteins and full virulence of
406 *Magnaporthe oryzae*. *Molecular Plant Pathology*. Doi:10.1111/mpp.12487.

407 Metz B, Kossen NWF, 1977. The growth of molds in the form of pellets–a literature
408 review. *Biotechnology and Bioengineering* **19**: 781-799.

409 Monosov EZ, Wenzel TJ, Luers GH, Heyman JA, Subramani S, 1996. Labeling of
410 peroxisomes with green fluorescent protein in living *P. pastoris* Cells. *Journal of*
411 *Histochememistry and Cytochemistry* **44**: 189-581.

412 Napolitano R, Juárez MP, 1997. Entomopathogenous fungi degrade epicuticular
413 hydrocarbons of *Triatoma infestans*. *Archives of Biochemistry and Biophysics* **344**: 208–14.

414 Pedrini N, Crespo R, Juárez MP, 2007. Biochemistry of insect epicuticle degradation by
415 entomopathogenic fungi. *Comparative Biochemistry and Physiology. Part C: Toxicology &*
416 *Pharmacology* **146**: 124–37.

417 Pedrini N, Mijailovsky SJ, Girotti JR, Stariolo R, Cardozo RM, Gentile A, Juárez MP,
418 2009. Control of pyrethroid-resistant Chagas disease vectors with entomopathogenic fungi.
419 *PLoS Neglected Tropical Diseases* **3**(5): e434.

420 Pedrini N, Zhang S, Juárez MP, Keyhani NO, 2010. Molecular characterization and
421 expression analysis of a suite of cytochrome P450 enzymes implicated in insect
422 hydrocarbon degradation in the entomopathogenic fungus *Beauveria bassiana*.
423 *Microbiology* **156**: 2549–2557.

424 Pedrini N, Ortiz-Urquiza A, Huarte-Bonnet C, Zhang S, Keyhani NO, 2013. Targeting of
425 insect epicuticular lipids by the entomopathogenic fungus *Beauveria bassiana*:
426 hydrocarbon oxidation within the context of a host-pathogen interaction. *Frontiers in*
427 *Microbiology* **4**:24.

428 Ryoo D, Choi CS, 1999. Surface thermodynamics of pellet formation in Aspergillus niger.
429 *Biotechnology Letters* **21**: 97–100.

Smith JJ, Aitchison JD, 2013. Peroxisomes take shape. *Nature Reviews Molecular Cell Biology* **14**: 803–817.

Tanaka A, Ueda M, 1993. Assimilation of alkanes by yeast: functions and biogenesis of peroxisomes. *Mycological Research* **97(9)**: 1025-1044.

Wang ZL, Zhang, LB, Ying SH, Feng MG, 2013. Catalases play differentiated roles in the adaptation of a fungal entomopathogen to environmental stresses. *Environmental Microbiology* **15(2)**:409-418.

Wucherpfennig T, Kiep KA, Driouch H, Wittmann C, Krull R, 2010. Morphology and rheology in filamentous cultivations. *Advances in Applied Microbiology* **72:** 89–136.

Xie XQ, Ying SH, Feng MG, 2010. Characterization of a new Cu/Zn-superoxide dismutase from *Beauveria bassiana* and two site-directed mutations crucial to its antioxidation activity without chaperon. *Enzyme and Microbial Technology* **46**: 217-222.

Xie XQ, Li F, Ying SH, Feng MG, 2012. Additive contributions of two manganese-cored superoxide dismutases (MnSODs) to antioxidation, UV tolerance and virulence of *Beauveria bassiana*. *PLoS One* **7(1)**: e30298.

Zhou YH, Zhang YJ, Luo ZB, Fan YH, Tang GR, Liu LJ, Pei Y, 2012. Selection of optimal reference genes for expression analysis in the entomopathogenic fungus *Beauveria bassiana* during development, under changing nutrient conditions, and after exposure to abiotic stresses. *Applied Microbiology and Biotechnology* **93**: 679–685.

451 **Figure legends**

452 **Fig. 1.** A) Mycelial pellets in aqueous solution in a test tube. B) Phase-contrast microscopy
453 of an isolated pellet formed by hyphae cumulates (40× magnification). C) Hexadecane
454 droplets surrounding the mycelial pellet (10× magnification). D) Mycelial pellet stained
455 with DAB (10× magnification). E) Mycelial pellet stained with DAB (20× magnification).

456

457 **Fig. 2.** Cell surface hydrophobicity of CM and MM-C16 conidia after 3, 5 and 7 days of
458 culture. * ($p < 0.05$), ** ($p < 0.01$).

459

460 **Fig. 3.** A) Optical observation of a semi-thin section of a mycelial pellet showing the
461 hyphal cumulate structure (40× magnification). B) Ultrastructure of mycelial pellets at
462 50,000× magnification. C) Ultrastructure of MM-C16 biomass at 30,000× magnification.
463 D) Ultrastructure of CM biomass at 30,000× magnification. E), F) Ultrastructure of
464 mycelial pellets at 30,000× magnification stained with DAB. The reaction appears as black
465 dots (white arrow), and several peroxisomes are visible. Hairpin-like structures are found in
466 the cell surface (black arrow). G), H) Ultrastructure of CM biomass at 30,000×
467 magnification stained with DAB. The reaction is positive mainly in vacuoles, and fewer or
468 none peroxisomes are visible. V: vacuole. N: nucleus. M: mitochondrium. P: peroxisome.

469

470 **Fig. 4.** Atomic force microscopy images of MM-C16 conidia (A, C, E) and CM conidia
471 (B, D, F) obtained in tapping mode. Images have a resolution of 512 x 512 pixels. The
472 height is expressed in color scale (right bar).

473

474 **Fig. 5.** Gene expression ratios of 3 days and 7 days of s of *B. bassiana* grown in MM-C16
475 or CM (control). A) Oxidative stress marker genes in mycelial pellets. B) Peroxin genes in
476 mycelial pellets. C) Hydrophobin genes in mycelial pellets (MP) and MM-C16 biomass.
477 Error bars represent standard errors of four independent assays. Dashed line showed a
478 relative expression ratio = 1. **($p < 0.01$), *** ($p < 0.001$).

Table 1. Oligonucleotides used in this study.

Name	Forward primer	Reverse primer	Efficiency (%)	R^2	Name/Function	Reference
Bbact	ATGGAGGAAGAAGTTGCTGC	ACACGGAGCTCGTTGTAGAA	112.7	0.992	γ-Actin	Zhou et. al. (2012)
Bbsod1	ACAACACCAACGGCTGCACC	ACGGCCAACAACGCTGTGAG	116	0.997	Cu/Zn- superoxide dismutase / O_2^- scavenging	Forlani et. al. (2014)
Bbsod2	CCAGTGTTTGGCATTGACATG	TCAGCCGTCTTCCAGTTGATG	105.6	0.996	Mn-superoxide dismutase / O_2^- scavenging	Forlani et. al. (2014)
Bbsod3	ACATCAATCACACTCTCTTCTG	GCGTTGGTCTGCTTCTTG	103.1	0.992	Mn-superoxide dismutase / O_2^- scavenging	Forlani et. al. (2014)
Bbgpx	CAAGGTCGTCCTCGTCGTCAAC	CTTGTCGCCATTGACCTCCACC	122.5	0.994	Glutathione peroxidase / GSH protection system	Forlani et. al. (2014)
Bbgst	TCTTGTAGCCAGCCCTCCATCG	AGAGATGTGGTCGCGGAACGA	115.5	0.969	Glutathione-S-transferase / GSH protection system	Forlani et. al. (2014)
Bbcata	GAAAGCCGCGCAAGTGAAAG	TCTCTGGCAAAGACATCCAG	107.2	0.993	Spore-specific catalase/ H_2O_2 scavenging	Forlani et. al. (2014)
Bbcatb	GAAGACGCCCATGTTTGTTCG	AAAGTTGCCCTCATCGGTATAGC	117.3	0.987	Secreted catalase/ H_2O_2 scavenging	Forlani et. al. (2014)
Bbcatc	TGCTGGACGATGTGTCTGAC	CACGCACCGTATCGCTAGAG	108.6	0.991	Cytoplasmic catalase/ H_2O_2 scavenging	Forlani et. al. (2014)
Bbcatd	GCGCTCGCAGTGACTGTAC	CTAGCACGGCCCTGTATAATGG	113.3	0.998	Secreted peroxidase/catalase / H_2O_2 scavenging	Forlani et. al. (2014)
Bbcatp	TGTACTGGGGCTCCGAACC	ATGAGACCTGTGTAGCGTTAGC	105.7	0.967	Peroxisomal catalase/ β-oxidation pathway	Forlani et. al. (2014)
Bbpex5	AATGCCGGGCCGAATATGC	CAGGCTGGCTGTTGAAATCGTG	130.2	0.991	Peroxisomal	This study

					biogenesis factor 5/ PTS1 import receptor	
Bbpex7	TCGCTTCGGCTGCCAATTTC	TGCGACAATGAGCTGGTTCTCG	111.1	0.993	Peroxisomal biogenesis factor 7/ PTS2 import receptor	This study
Bbpex14/ 17	TCGCCAACCTCGTCAGACACTG	CCTCGACGCCCTTTGACTTGAG	114.3	0.991	Peroxisomal biogenesis factor 14/17/ Receptor docking complex	This study
Bbpex19	AAGTTCCCTGTCTGGCTGTCGG	CCGGCAAAGGCTTCTTGTGC	114.3	0.993	Peroxisomal biogenesis factor 19/ soluble chaperone and receptor	This study
Bbhyd1	CACCATGGTGGAAAGGATCTGCAC	CCGAGAAGGTGGGAAAGAAGACCA	108.5	0.996	Hydrophobin 1 / cell surface hydrophobicity	This study
Bbhyd2	TGTCAAGACTGGCGACATTTGCG	TCGATGGGGACAAGCTGGTTGA	117.7	0.985	Hydrophobin 2 / cell surface hydrophobicity	This study

Table 2. Determination of humid biomass ratio and pH of the remaining media at different time periods. For both assays, values in each column followed by different lowercase letters and values in each line followed by different uppercase letters indicate significant differences ($p<0.05$).

Day	Biomass ratio		pH	
	MM-C16	CM	MM-C16	CM
3	1.2 ± 0.2aA	6.1 ± 0.8aB	6.1 ± 0.4aA	3.6 ± 0.1aB
5	1.2 ± 0.2aA	7.4 ± 1.4aB	5.4 ± 0.7aA	6.5 ± 0.1bA
7	1.1 ± 0.3aA	5.4 ± 1.9aB	4.9 ± 0.5aA	7.1 ± 0.1cB

Table 3. Pathogenicity bioassay. Cumulative percentage mortality ± SEM of *Tribolium castaneum* and *Tenebrio molitor* larvae treated with *Beauveria bassiana* mycelial pellets and corrected for control mortality using the Abbott's formula. For both insects, different letters indicate significant differences ($p < 0.05$).

Day	Mortality (%)	
	Tribolium castaneum	*Tenebrio molitor*
0	0 ± 0a	0 ± 0a
2	0 ± 0a	0 ± 0a
5	70.2 ± 11.9b	53.3 ± 10.7b
8	67.3 ± 13.1b	96.7 ± 1.9c

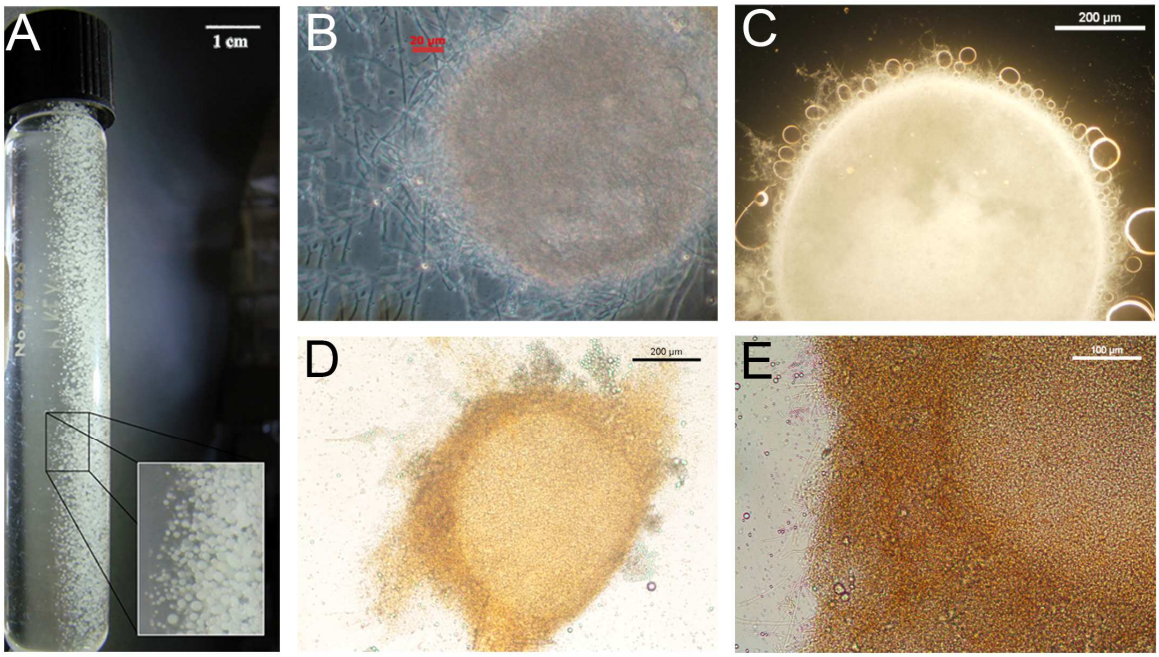

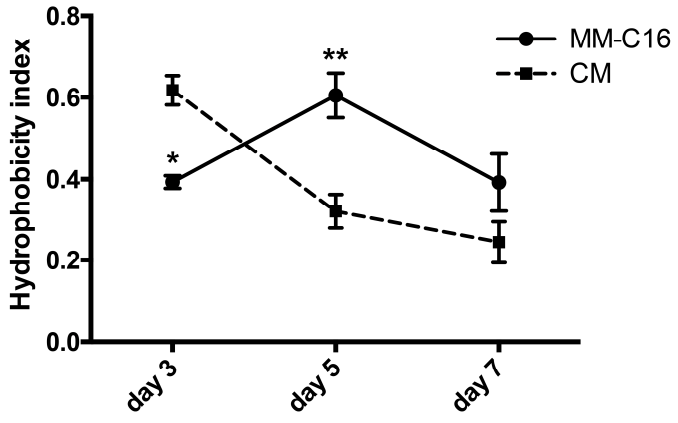

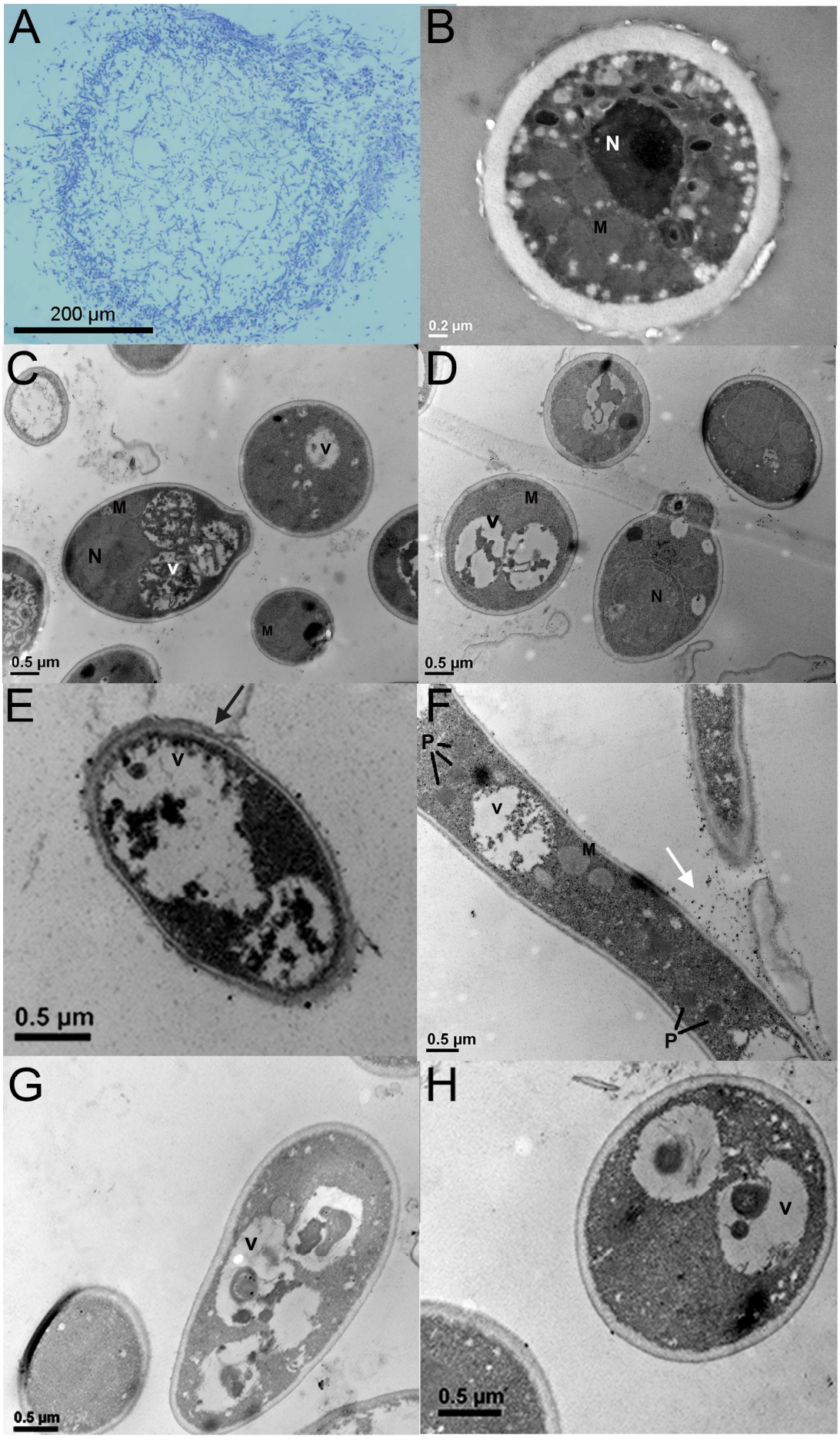
A
200 µm
B
N
M
0.2 µm
C
V
M
N
V
M
0.5 µm
D
M
V
N
0.5 µm
E
V
0.5 µm
F
P
V
M
P
0.5 µm
G
V
0.5 µm
H
V
0.5 µm